2025 Journal of Engineering, Technology and Social Sciences
Jurnal Kejuruteraan, Teknologi dan Sains Sosial
Volume 11 Special Issue: ICoSCiD
International Conference on Smart Cities Development
e-ISSN: 27166848

LARGE-SCALE TOPOGRAPHIC MAPPING USING UAV PHOTOGRAMMETRY

Norina Omar[1], Fauzul Azhan Abdul Aziz[2] and Nurin Uzma Dini Sahrul Nizam[3]

[1,2]*Department of Civil Engineering, Ungku Omar Polytechnic, Perak, Malaysia*
[3]*Perkhidmatan Jurukur S Sepakat Sdn.Bhd, Ipoh Perak, Malaysia*
[*]*omar.norina@gmail.com*

ARTICLE INFO

Article history:
Received
14 July 2025
Received in revised form
10 August 2025
Accepted
3 Oct 2025
Published online
15 Oct 2025

Keywords:
Unmanned Aerial Vehicle (UAV);
Structure from Motion (SfM);
Multi-View Stereo (MVS);
Orthomosaic;
Digital Terrain Model (DTM);
topographic map;
large scale

ABSTRACT

Topographic maps provide essential information for various applications, including infrastructure planning, land surveying, and disaster management. Various methods are available to produce topographic maps, ranging from traditional ground surveying to advanced remote sensing techniques. However, each approach has notable limitations. Ground surveying is time-consuming and labor-intensive, LiDAR systems are often restricted by high costs and operational complexity, and satellite imagery is affected by cloud cover and has lower spatial resolution compared to LiDAR and UAV data. These challenges highlight the need for efficient, accurate, and cost-effective alternatives methods. This study evaluates the effectiveness of UAV photogrammetry in producing large-scale topographic maps by assessing the horizontal and vertical accuracy of orthomosaics and DTMs, as well as analyzing their visual quality. The study site is located at the Ungku Omar Polytechnic, Perak, Malaysia. The DJI Mavic 2 Pro was used to collect digital aerial images, aided by the 3Dsurvey Pilot flight planning apps. Orthomosaics and DTMs were generated using Agisoft Metashape Professional. The findings revealed sub-meter positional accuracy, with $RMSE_H$ and $RMSE_V$ values of 0.217 m and 0.227 m, respectively. UAVs in conjunction with SfM-MVS photogrammetry may produce reliable and precise topographic mapping, supporting broader adoption of UAV technology in geospatial applications.

1. Introduction

The need for precise spatial data to support informed decision-making in crucial areas like urban planning, infrastructure development, environmental monitoring, and disaster management has led to a significant increase in demand for accurate and current topographic maps in recent years. A topographic map depicts a detailed and precise geometric representation of both natural and man-made features on the ground, such as roads, railways, pipelines, power transmission lines, buildings, contours, elevations, rivers, lakes, and many others. This map is essential since it provides an information on the actual situation on the ground in certain areas and is regarded as one of the most significant maps utilized by all

organizations, including the military, government, business sector, and individuals (Muhammad & Tahar, 2021). It also acts as a vital base reference for geospatial data in rapid emergency response and mapping applications (Pathak et al., 2024).

Various techniques are available for executing topographic mapping, evolving from ground surveying methods to modern, technology-driven ones. Each approach offers distinct preferences and encounters limitations based on the scale, accuracy, and terrain characteristics of the study area. The ground surveys and manned aerial photogrammetry have long served as the foundation for producing accurate topographic maps. The use of total station surveys, leveling, and GNSS remains important for applications that require high precision but are restricted to small areas, labor-intensive, time-consuming, affected by weather conditions, and challenging due to terrain accessibility, especially in rugged remote and dense urban areas. Besides, less suitable for large-scale or complex areas where speed and efficiency are needed. Meanwhile, the manned aircraft method can cover large areas but involves high operational costs, requires complex logistics, and has limited flexibility for rapid data collection in dynamic environments.

In contrast, advanced options such as Light Detection and Ranging (LiDAR), satellite remote sensing and Unmanned Aerial Vehicle (UAV) photogrammetry have revolutionised the efficiency and accuracy of topographic data collection (Du et al., 2022). LiDAR provides highly accurate three-dimensional elevation data, capable of penetrating vegetation to extract bare-earth models, making it ideal for forested and complex landscapes. However, it has a major drawback due to the high operational cost, which requires high-end software, robust hardware, and skilled personnel for data processing. Meanwhile, satellite-based remote sensing enables broad-scale topographic mapping. Nonetheless, it typically provides lower spatial resolution images than UAV and LiDAR data and is frequently impacted by cloud cover, particularly in tropical regions. Based on these limitations associated with ground surveying methods, remote sensing satellite and LiDAR, this study evaluates the capability of UAV photogrammetry in generating large-scale topographic maps by assessing the positional accuracy of derived products and examining the visual quality of orthomosaic and Digital Terrain Models (DTM).

1.1 Unmanned Aerial Vehicle (UAV) Photogrammetry

Currently, the introduction of UAVs or drones has offered certain functionalities that contribute to their widespread utilisation in geospatial applications(Muradás Odriozola et al., 2024). UAVs may be categorised into four classes based on their take-off mechanism: single rotor, multi rotor, fixed wing, and hybrid VTOL. This aircraft system uses an advanced navigation system and high-resolution cameras or other payloads to operate without a human pilot, passengers, or crew on board. Their ability to capture high-resolution imagery quickly at relatively low cost in various altitudes and angles, and high temporal flexibility, allowing for precise data collection even in complex or hard-to-reach terrains (Quamar et al., 2023). In addition, they are a cost-effective alternative to manned aerial systems, which makes them a desirable choice for both small and large-scale mapping projects (Cho et al., 2021). According to Zolkepli et al. (2023), a multirotor UAV has shown greater efficacy in slope mapping. The slope measurements, such as its perimeter, area, and volume, can be obtained quickly and

precisely from the mapping outputs, such as DEM and orthophoto.

Photogrammetry is the science of making measurements from photographs and is widely used for spatial data acquisition, particularly in mapping applications (Saifizi et al., 2020). It has become more popular in recent years due to the parallel growth of commercially accessible drone hardware and user-friendly software (Rábago & Portuguez-Castro, 2023). The integration of UAVs with Structure from Motion (SfM) photogrammetry facilitates the processing of multiple overlapping images through the detection and matching of common features, enabling the generation of a sparse 3D point cloud. This robust approach further the generation of highly realistic 3D models and accurate geospatial outputs through the application of multi-view stereo (MVS) techniques. However, parameters such as flight altitude, flight planning apps, sensor or camera quality, types of UAV used, percentage of image overlap, camera calibration, processing techniques, terrain variability, ground sampling distance (GSD), and the placement of Ground Control Points (GCPs) substantially affect the accuracy and reliability of data outputs.

The adoption of UAV photogrammetry remains a critical research concern for geospatial researchers, as they may face uncertainties. Santrač et al. (2023) investigated the quality of digital orthophoto and Digital Surface Model (DSM) in terms of the RGB or multispectral sensor used, multi-altitude flights, flight paths, and the arrangement of GCPs. Meanwhile, Bulut & Yılmaztürk (2022) examined how accurate orthomosaic and DEM are based on different height, angle, and overlap ratios by using two different processing software programs, Agisoft Metashape and Pix4D Mapper. Syetiawan et al. (2020) showed that the direct georeferencing approach can produce high accuracy topographic maps for relatively not extensive site areas.

Therefore, assessing a geospatial product's accuracy still requires a thorough evaluation to ensure compliance with the mapping standards. Thus, this research aims to evaluate the capabilities of employing a multirotor UAV integrated with photogrammetry methods for large-scale topographical mapping. This study used an UAV equipped with RGB camera to capture aerial images, involve Ground Control Points (GCPs) measurement using GNSS equipment, image processing using SfM-MVS techniques to produce 2D maps and 3D models of the terrain, and finally perform features extraction and data analysis using GIS software. The accuracy of orthophotos and DTM were also evaluated both quantitatively and qualitatively before the production of topographic maps.

2. Materials and Methods

The study is divided into four (4) major phases: the first phase involves a preliminary study, such as selection of study area, software, arrangement of GCPs, and equipment selection, including UAV platform types and flight planning apps. The second phase is field data collection of UAV images and GNSS data measurement of GCPs. The third phase involves data processing to generate photogrammetric outputs, and the last phase involves data analysis and conclusion. Figure 1 shows the research study's workflow.

2.1 The Study Area

A study area is located around the Ungku Omar Polytechnic in Ipoh, Perak, Malaysia as shown in Figure 2. The approximate coordinates in the WGS84 geodetic reference system are 101° 7' 24.3546" N and 4° 35' 18.6576" E. The total area of this site is about 61.4 acres or 0.25 km^2. This study area was selected because it contains road networks, green spaces, water bodies, open spaces, and built-up areas.

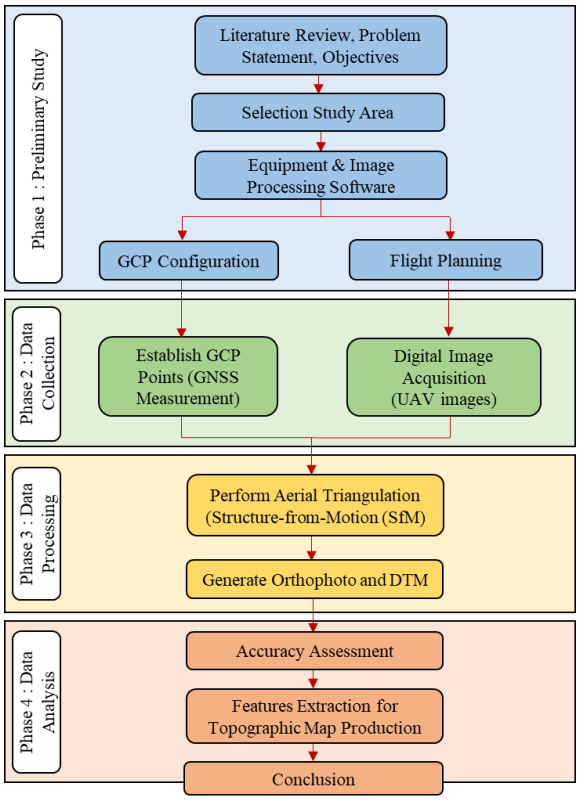

Figure 1. Flowchart of Research Methodology

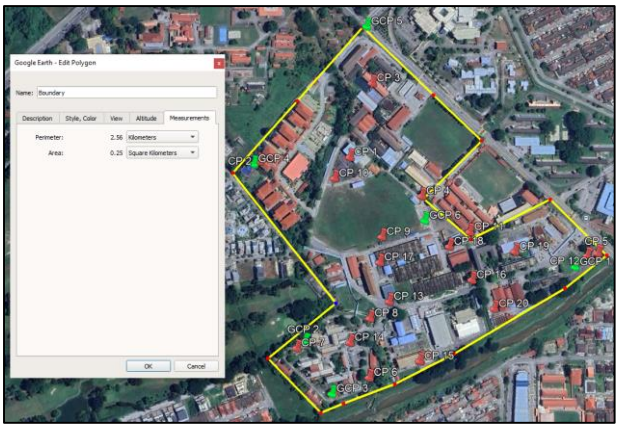

Figure 2. The study area with Ground Control Points (GCPs) and Check Points (CPs) distribution.

2.2 Establishment of Ground Control Points

A total of six Ground Control Points (GCPs) were established around the study area and precisely measured using the CHCNAV i50 Global Navigation Satellite System (GNSS) receiver. The Rapid Static survey method was employed, with approximately 30 minutes of observation per point at a 1-second interval. The detailed specifications of the GNSS equipment used for data collection are presented in Table 1, while Table 2 summarizes the GNSS parameters for data observation. All the pre-mark control points are systematically distributed over the study area, and they were used to improve exterior orientation and the overall accuracy level of the photogrammetric model (Alias et al., 2022). Liu et al. (2022) suggest that GCPs should be uniformly dispersed around the research area, with a minimum of one GCP located in the middle of the domain. Although the preparation and measurement of GCPs demand considerable time and effort, this method is advisable for achieving higher quality results (Elkhrachy, 2021).

Table 1. Specifications of the CHCNAV i50 RTK GNSS Receiver

Parameter	Specification
GNSS Constellations	GPS, GLONASS, Galileo, BeiDou, QZSS, SBAS
Frequency used	Dual Frequency (L1, L2)
Positioning Accuracy	Horizontal static: 3 mm + 0.5 ppm Vertical static: 5 mm + 0.5 ppm
Positioning rate	Up to 10 Hz
Ephemeris	Broadcast
UHF Range	Up to 5 km
Communication	Bluetooth, Wi-Fi, 4G modem, internal UHF radio

Table 2. Parameters for GNSS observation with the Rapid Static method

Field Parameter	Settings
Observation Information	Carrier phase (dual-frequency minimum)
Durations of Observations	30 minutes
Observation interval	1 second
Number of satellites	Minimum six (6) satellites
Elevation angle cut-off angle	15 degrees
PDOP value	Maximum seven (7)
Centering of antenna	Above the earth control point
Antenna Height	2.0 meters

To ensure the GCPs' visibility in collected photographs during UAV flights, control points of 120 cm x 120 cm in square black and white were positioned in open and flat areas, clear of obstructions such as trees, buildings, and structures. Figure 3 shows a GCP setup at the target site. The cross marker makes the GCP visually identifiable in the UAV images to link the GNSS position with the image pixels. The GNSS raw data was processed using Trimble Business Center (TBC) software to obtain the final coordinates of GCPs in the Geodetic Datum of Malaysia 2000 Perak coordinate system. Table 3 shows the results of Ground Control Point (GCP) post-processing, where a Continuously Operating Reference Station (CORS) at Pusing,

Perak (PUSI) was chosen to correct the GNSS receiver positions. The table summarizes fixed solution GCPs with horizontal precision ranging from 0.009 to 0.025 meters, vertical precision from 0.014 to 0.028 meters, and RMSE values of 0.023 to 0.034 meters. The maximum Position Dilution of Precision (PDOP) values are between 1.417 and 1.944, indicating better satellite geometry and good positional accuracy.

Table 4 presents the surveyed GCPs used for georeferencing UAV imagery. Each GCP includes easting, northing, and elevation values in a projected coordinate system, as well as geographic coordinates in degrees-minutes-seconds format. These points serve as spatial references for aerial triangulation in the photogrammetric processing workflow. Their precise coordinates ensure that the desired photogrammetric products accurately align with real-world positions. Additionally, twenty (20) Check Points (CPs) were obtained from previous GNSS surveyed data measurements to evaluate the positional accuracy of orthophotos and DTM.

Figure 3. Ground control point installation at the target site.

Table 3. Ground Control Point processing results.

Observation	Solution Type	H. Prec. (m)	V. Prec. (m)	RMS	Max PDOP
PUSI - GCP1	Fixed	0.011	0.017	0.023	1.588
PUSI - GCP2	Fixed	0.025	0.028	0.025	1.708
PUSI - GCP3	Fixed	0.015	0.022	0.026	1.790
PUSI - GCP4	Fixed	0.010	0.021	0.027	1.944
PUSI - GCP5	Fixed	0.010	0.020	0.034	1.562
PUSI - GCP6	Fixed	0.009	0.014	0.024	1.417

Table 4. GCPs measured using CHCNAV i50 GNSS receiver.

Point ID	Easting (m)	Northing (m)	Elevation (m)	Latitude	Longitude	Ellipsoidal Height (m)
GCP1	34501.866	-29936.018	45.974	N4°35'17.831"	E101°07'34.801"	39.228
GCP2	33954.899	-30086.771	44.972	N4°35'12.931"	E101°07'17.054"	38.197
GCP3	34020.555	-30183.803	44.753	N4°35'09.771"	E101°07'19.183"	37.983
GCP4	33871.056	-29747.605	49.376	N4°35'23.974"	E101°07'14.339"	42.591
GCP5	33871.056	-29484.182	49.455	N4°35'32.546"	E101°07'21.311"	42.679
GCP6	34192.889	-29829.390	45.843	N4°35'21.307"	E101°07'24.779"	39.078

2.3 Flight Planning and UAV Image Acquisition

The DJI Mavic 2 Pro, a multirotor, was used to collect aerial image data. The UAV equipment was calibrated using the DJI GO 4 application before data acquisition, generally focusing on compass, camera, and IMU calibration to ensure optimal flight performance and good image quality during flight operations. The flight plans were prepared and executed by using the 3Dsurvey Pilot application on a mobile phone and connected to the drone. Autonomous UAV flights were conducted along a pre-designed flight path at a speed of approximately 3 m/s with a flight altitude of 85 meters above ground level, and the camera angle was set to 90° (vertical). The setting parameter for forward overlap was 80%, and the side overlap was 70%. The ground sample distance (GSD) was 1.93 cm with image resolution 5472 x 3648 pixels. A total of 747 aerial photographs were obtained with four (4) flight phases on the same day. The flight time for the entire survey area took about 1 hour, 19 minutes, and 30 seconds.

2.4 Image Processing

Agisoft Metashape Professional 2.0.2 was applied to generate photogrammetric products from collected aerial images, such as dense point clouds, Digital Elevation Model (DEM), Digital Terrain Model (DTM), contour lines, and orthomosaic. The process of aerial triangulation, including image matching, aligning, and bundle adjustment, was carried out in this software. The coordinate system used for UAV data processing is based on the Geodetic Datum of Malaysia 2000/ Perak Grid. Figure 4 outlines a photogrammetric processing workflow using UAV images with GCPs. It begins with adding all the images collected into the Agisoft Metashape software and estimating their image quality by using a tool called Estimate Image Quality. As a results, the image quality score is ranged from 0.50 to 0.99, with a mean score of 0.82. The quality score for image under 0.50 units should be removed from the photo alignment process to improve the accuracy of the photogrammetric outputs (Agisoft LLC, 2023). Images with lower scores tend to be blurred or poorly exposed, which can cause incorrect camera alignment and lead to errors and inconsistencies in the resulting 3D model.

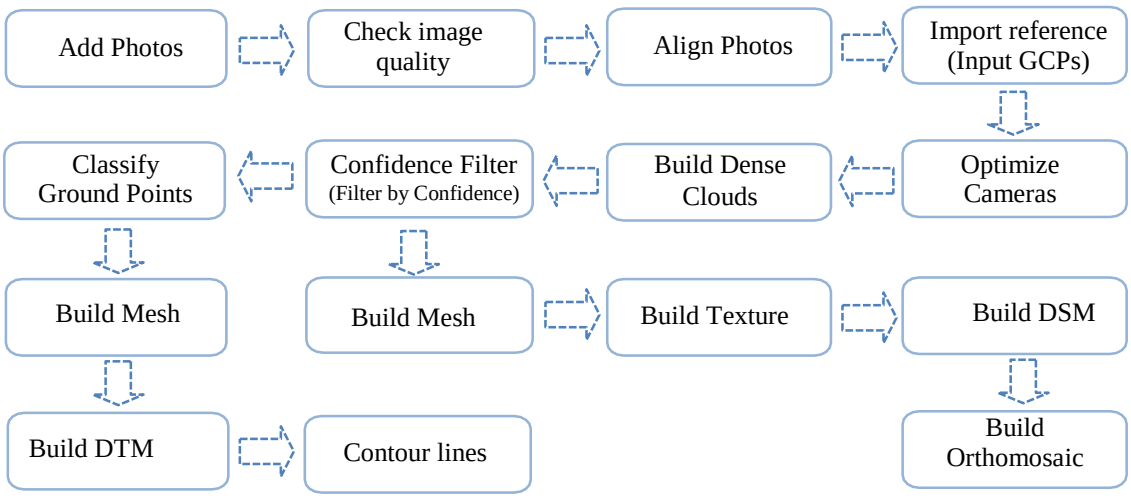

Figure 4. Processing flow of UAV images with GCPs

After that, the photos were aligned to generate a sparse point cloud using the Align Photos function. This process identifies and matches common features (tie points) from two or more overlapping photos to reconstruct the initial 3D geometry. GCPs were imported and marked to improve the model's georeferencing accuracy. This was followed by camera optimization, which refines the internal and external camera parameters to minimize errors and increase the overall precision of the model. The internal camera parameters refer to the geometric and optical characteristics of the camera sensor, such as focal length, principal point coordinates, and lens distortion coefficients. The external camera parameters describe the camera's orientation and position in space at the time of image capture, the rotation angles (roll, pitch, yaw), and translation components (X, Y, Z).

A dense point cloud was generated using the Build Point Cloud function with medium quality settings and mild depth filtering, employing the Multi-View Stereo (MVS) algorithm. These points were filtered by confidence to remove unreliable data to ensure the quality and efficiency of subsequent model processing. DTM and orthomosaic are generated for accurate geospatial representation and further analysis. To create a DTM, ground points were classified from a dense point cloud under automated tool Classify Ground Points. The contour line was extracted from the DTM using the Generate Contour tools. Finally, the production of the topographic map was prepared after all the spatial data had been processed and validated. These datasets were combined and symbolized appropriately in a CADD environment to produce a comprehensive topographic map that accurately depicts the terrain and features of the study area.

2.5 Accuracy Assessment

The accuracy assessment of the orthomosaic and Digital Terrain Model (DTM) was conducted by employing both quantitative and qualitative analysis. For quantitative evaluation, independent checkpoints (CPs) were used to quantify the horizontal and vertical positional accuracy through the calculation of the Root Mean Square Error (RMSE), based on the Accuracy Standards for Digital Geospatial Data (ASPRS) Positional Accuracy Standards (2024). This involved comparing the coordinates obtained from the generated geospatial product with the actual observed values of the CPs. The computed RMSE values provided a statistical indicator of the overall spatial accuracy of the dataset. A lower RMSE indicates higher positional accuracy and good alignment with the ground truth data, which confirms the reliability of the desired outputs. In addition, the $RMSE_H$ was computed for the easting (X), northing (Y), and vertical (Z) coordinates, as well as the total $RMSE_Z$. Meanwhile, qualitative analysis involves a visual inspection and interpretation of the photogrammetric output's appearance. This includes checking the alignment of visible objects such as roads and buildings to ensure they appear correctly positioned and undistorted. For the DTM, surface features are checked for smoothness, continuity, and the realistic representation of terrain.

3. Results and Discussion

3.1 Accuracy of Indirect Georeferencing

Table 5 shows the Root Mean Square Error (RMSE) values for six control points used to evaluate the indirect georeferencing performance of the photogrammetric model in Agisoft Metashape. The Easting (X), Northing (Y), and Altitude (Z) error values for all GCPs were minimal, with the majority of the errors being less than 1 cm. The RMSE for the control points was calculated as 0.524 cm, 0.733 cm, and 0.0096 cm in X, Y, and Z direction, respectively, resulting in a total 3D positional $RMSE_{GCP}$ of 0.901 cm. Each GCP was projected onto between 9 and 16 images, contributing to enhanced spatial redundancy and improving georeferencing reliability.

Additionally, the reprojection error for the six GCPs was below 0.5 pixels, with an average of 0.311 pixels, indicating precise alignment between the image coordinates and the model geometry. The derived values demonstrate a high level of positional accuracy achieved through the integration of GCPs, which confirms the reliability of photogrammetric outputs. The orthomosaic and Digital Terrain Model (DTM) derived from using SfM-MVS photogrammetric techniques are appropriate for large-scale topographic mapping and geospatial analysis applications. These results are consistent with those of Ahmed et al. (2022) who indicated that the indirect georeferencing approach in UAV photogrammetry can achieve high positional accuracy, with RMSE values reduced to a few centimetres. This reinforces the effectiveness of using GCPs in enhancing spatial precision. Contrarily, the results also highlight that direct georeferencing using low-cost UAVs tends to yield lower accuracy geospatial outputs, even when flown at low altitudes.

Table 5. Control points RMSE

Label	X error (mm)	Y error (mm)	Z error (mm)	Total (mm)	Image (pix)
GCP1	-2.054	2.051	-0.014	2.903	0.227 (9)
GCP2	-2.406	-11.875	0.137	12.117	0.312 (13)
GCP3	-6.544	9.073	-0.078	11.187	0.411 (12)
GCP4	-1.612	-5.770	-0.162	5.993	0.295 (10)
GCP5	2.478	-1.304	0.018	2.800	0.311 (13)
GCP6	10.159	7.737	0.042	12.770	0.271 (16)

3.2 Orthomosaic, DSM and DTM

The Digital Surface Model (DSM) presented in Figure 5(a) provides a detailed representation of the study area's surface with elevation values ranging from 11 meters to 74 meters. The variations in elevation are highlighted by the color distribution, which displays higher elevation levels in red and lower areas in blue. This product included both natural and man-made objects such as buildings, trees, and other infrastructure. It is important to note that DSMs do not directly provide bare-earth ground elevation. Therefore, the ground filtering process must be performed to extract accurate ground elevation (Z)

values from a raw dense 3D point cloud. Jiménez et al., (2021) emphasize the importance of ground filtering process to yield an accurate land surface model that truly represents the bare earth surface.

The generated DTM as shown in Figure 5(b), represents the elevation model of the ground surface with color gradients indicating variations in terrain height within the study area. The elevation values specifically range from 12.6 meters to 52.3 meters above orthometric height. Lower elevation areas were shown in shades of blue and green hues, while higher elevations are represented in yellow to red tones. This elevation data was automatically derived from a dense point cloud classification by removing above-ground features such as buildings and vegetation, thereby reducing manual effort required and decreasing overall processing time.

Figure 5(c) presents a high-resolution orthomosaic image that is geometrically corrected, which is a true-to-scale visual representation of the study area. Object features such as roads, buildings, and vegetated regions are clearly identifiable and well-aligned, indicating successful image stitch and spatial referencing based on Ground Control Points (GCPs). The accuracy of the orthophoto with 1.85 cm GSD in this study is consistent with previous findings by Pathak et al. (2024), who assured that a high-resolution orthophoto suitable for extracting topographic features to support the production of topographic maps.

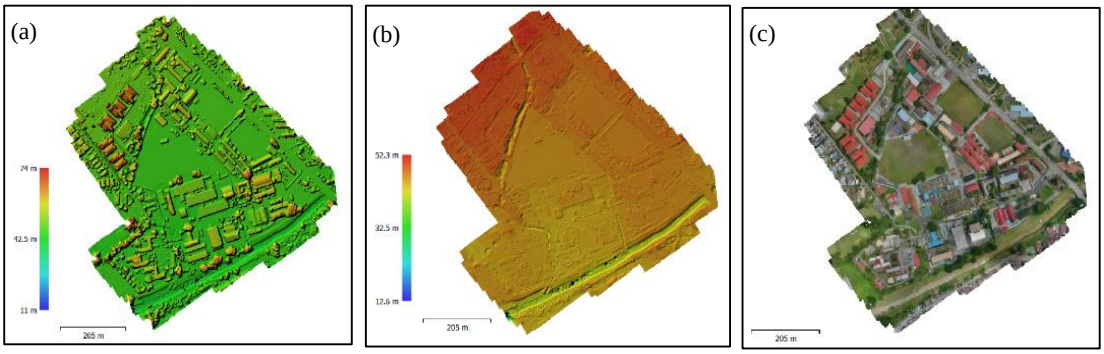

Figure 5. Digital Surface Model (a) Digital Terrain Model (b) and Orthomosaic (c)

3.3 Quantitative Assessment, Positional Accuracy

Table 6 presents a comparison between map-derived values and GNSS-measured values at checkpoints (CPs) for 20 control points, indicating the high positional accuracy of the created model. The mean errors for the X, Y, and Z coordinates are -0.027 m, 0.018 m, and -0.070 m, respectively, indicating minimal systematic bias. The standard deviations are 0.106 m (X), 0.192 m (Y), and 0.222 m (Z), reflecting low variability in the residuals. The RMSEs are 0.107 m (X), 0.188 m (Y), and 0.227 m (Z), indicating that the differences between the map-derived and surveyed values are less than 1 meter, which supports higher accuracy. The horizontal and vertical RMSE values for checkpoint fits are 0.217 m and 0.227 m, respectively, further approving the model's suitability for accurate topographic mapping. Overall, these results show that the mapping workflow produces reliable and precise spatial data.

Table 6. Comparison of coordinates between GNSS-surveyed checkpoints and UAV-derived product values.

CP ID	Map Derived Values (meter)			Surveyed Checkpoints Values (meter)			Residuals (Error) (meter)		
	Easting (E)	Northing (N)	Elevation (Z)	Easting (E)	Northing (N)	Elevation (Z)	ΔE	ΔN	ΔZ
CP1	34057.259	-29733.817	46.143	34057.308	-29733.986	46.158	-0.049	0.169	-0.015
CP2	33882.042	-29742.401	49.393	33882.100	-29742.313	49.275	-0.058	-0.088	0.118
CP3	34093.098	-29498.119	48.799	34093.223	-29498.074	48.661	-0.125	-0.045	0.138
CP4	34200.966	-29815.656	45.760	34201.036	-29815.590	45.716	-0.070	-0.066	0.044
CP5	34525.158	-29923.758	45.769	34525.180	-29923.813	45.940	-0.022	0.055	-0.171
CP6	34056.030	-30182.877	44.292	34056.083	-30182.917	44.527	-0.053	0.040	-0.235
CP7	33952.088	-30097.782	44.289	33952.070	-30097.663	44.867	0.018	-0.119	-0.578
CP8	34130.725	-30100.096	44.000	34130.859	-30100.200	44.708	-0.134	0.104	-0.708
CP9	34013.229	-29883.962	45.661	34013.376	-29883.759	45.690	-0.147	-0.203	-0.029
CP10	34027.349	-29749.685	45.947	34027.324	-29749.516	45.906	0.025	-0.169	0.041
CP11	34254.112	-29847.732	45.850	34254.012	-29847.748	45.893	0.100	0.016	-0.043
CP12	34514.027	-29924.591	39.276	34514.048	-29924.614	39.294	-0.021	0.023	-0.018
CP13	34131.293	-30011.975	44.257	34131.492	-30011.868	44.406	-0.199	-0.107	-0.149
CP14	34057.523	-30089.362	45.064	34057.604	-30089.385	44.920	-0.081	0.023	0.144
CP15	34178.466	-30130.620	43.887	34178.367	-30131.153	43.735	0.099	0.533	0.152
CP16	34292.500	-29970.391	44.899	34292.626	-29970.026	44.981	-0.126	-0.365	-0.082
CP17	34114.744	-29940.110	44.681	34114.734	-29940.289	44.682	0.010	0.179	-0.001
CP18	34247.356	-29909.784	44.830	34247.426	-29909.984	44.839	-0.070	0.200	-0.009
CP19	34366.568	-29916.524	46.203	34366.334	-29916.455	46.209	0.234	-0.069	-0.006
CP20	34331.209	-30024.954	45.512	34331.077	-30025.198	45.511	0.132	0.244	0.001
					Number of Check Points		20	20	20
					Mean Error (m)		-0.027	0.018	-0.070
					Standard Deviation (m)		0.106	0.192	0.222
					RMSE (m)		0.107	0.188	0.227
					Fit to Checkpoint $RMSE_H$			0.217	
					Fit to Checkpoint $RMSE_Z$			0.227	

3.4 Qualitative Assessment, Visual Inspection of Orthomosaic and DTM

Figure 6 displays an orthomosaic image overlaid on a base map, Google Road, in QGIS software. This overlay allows for a direct visual comparison between the orthomosaic and the underlying map, which is useful for assessing spatial accuracy and the quality of the orthomosaic image. The orthomosaic shows high spatial accuracy, as evidenced by the close alignment of buildings, road intersections, and rivers with the Google base layer. There are no visible misalignments or distortions, no missing areas, and the object features in the orthomosaic can also be seen clearly. Furthermore, the image has uniform color and brightness throughout, with no visible seams or sudden changes between stitched photos. This shows good blending, making the orthomosaic image visible. Thus, indicating that the orthomosaic is well-georeferenced and reliable for geospatial analysis and mapping applications.

Figure 6. Orthomosaic overlay with Google Road in QGIS.

Based on Figure 7, which presents orthomosaic, DEM, and DTM images (horizontally) for three different land cover types: (a) dense buildings, (b) dense vegetation, and (c) flat areas. The generated DTM provides a reliable representation of the ground surface, especially in flat and open areas. In areas with dense buildings or vegetation, the DTM productively reduces above-ground features but may retain some residual objects. The visual assessment indicates that the DTM exhibits the highest quality in unobstructed areas, with minimal noise and clear surface depiction. In contrast, some refinement may be needed in densely built or vegetated regions to further minimize non-ground objects. Overlaying the DTM layer with the orthomosaic and DEM helps validate that above-ground features are removed appropriately, and the terrain morphology is captured realistically.

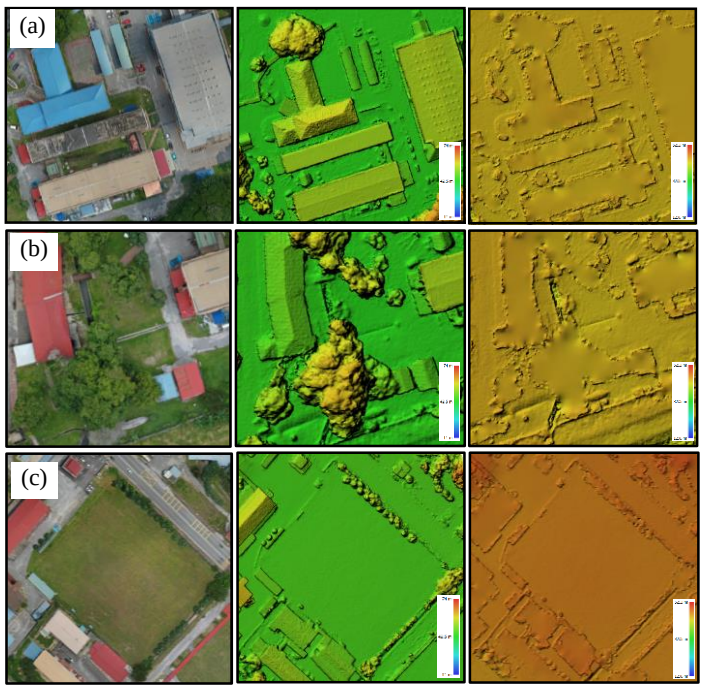

Figure 7. Orthomosaic, DEM and DTM respectively for (a) dense buildings, (b) dense vegetation and (c) flat areas.

3.5 Topographic Map

The production of the topographic map began with the digitization of object features within QGIS software by utilizing the orthomosaic generated from UAV images. Contour lines with a 5-meter interval were generated from the Digital Terrain Model (DTM) to represent elevation variations accurately. Further refinement of the topographic map was conducted using AutoCAD software to enhance precision and presentation quality. Figure 8 illustrates the finalized topographic map at a scale of 1:1700, produced through photogrammetric techniques applied to UAV imagery.

Figure 8. Topographic map of the study area.

4. Conclusion

This study presents an analysis of the use of a multirotor UAV for the production of large-scale topographic mapping at Ungku Omar Polytechnic, Perak, demonstrating the effectiveness of UAV photogrammetry in such applications. Two types of analysis, quantitative and qualitative, were carried out to assess the capability of UAV photogrammetry using Structure-from-Motion (SfM) and Multi-View Stereo (MVS) techniques in Agisoft Metashape Professional software. The quantitative analysis focused on positioning accuracy, while the qualitative assessment examined the visual quality and reliability of the photogrammetric outputs.

The analysis found that the positioning accuracy generated by UAV photogrammetry was compared with GNSS value, indicating that the RMSE for horizontal and vertical directions were 0.217 m and 0.227 m respectively, which less than 1 meter. The use of Ground Control Points (GCPs) significantly improves the positional accuracy of UAV-derived data, particularly for low-cost UAV platforms that are not equipped with Real-Time Kinematic (RTK) functionality. Their input is essential for achieving reliable results in high-precision mapping applications.

Qualitative analysis through visual inspection indicated that the orthomosaic product closely coincides with the Google base map, while the derived Digital Terrain Model (DTM) provides a reliable representation of the ground surface, especially in flat and open areas. However, in complex environments such as dense infrastructure or vegetation, further enhancement may be necessary to restrain the remaining non-ground objects. To overcome this matter, manual classification of the dense point cloud is recommended, particularly in areas where automated filtering fails to distinguish ground and non-ground features effectively.

Overall, the results confirm that the UAV imagery processed through Agisoft Metashape Professional provides reliable and accurate outputs for topographic mapping. Furthermore, the UAV-based approach offers significant benefits, including reduced processing time to prepare a topographic map, expanded area coverage capability, and decreased human intervention. These findings align with the study research of Abu Sari et.al (2020), which demonstrated that UAV photogrammetry is a workable alternative for updating topographic maps. In conclusion, the findings highlight that the potential of low-cost UAV platforms, when supported by appropriate processing workflows, is capable of delivering accurate and high-quality geospatial data suitable for topographic mapping applications.

Acknowledgements

The authors gratefully acknowledge the financial support from Ungku Omar Polytechnic, Ipoh, Perak, Malaysia, and Perkhidmatan Jurukur S. Sepakat Sdn. Bhd., as well as the provision of facilities that enabled the successful completion of this research.

References

Abu Sari, Mohd Yazid; Ahmad, Asmala;Yana Mazwin, Mohmad Hassim;Sahib, Shahrin; Abu Sari, Nasruddin ; Rasib, A. W. (2020). Large Scale Topographic Map Comparison Using Unmanned Aerial Vehicle (UAV) Imagers and Real Time Kinematic (RTK). *International Journal of Advanced Trends in Computer Science and Engineering*, *9*(1), 328–338.

https://doi.org/https://doi.org/10.30534/ijatcse/2020/5691.12020

Agisoft LLC. (2023). *Agisoft Metashape User Manual Professional Edition, Version 2.0*. Retrieved from **https://www.agisoft.com/pdf/metashape-pro_2_0_en.pdf**

Ahmed, S., El-Shazly, A., Abed, F., & Ahmed, W. (2022). The Influence of Flight Direction and Camera Orientation on the Quality Products of UAV-Based SfM-Photogrammetry. *Applied Sciences (Switzerland)*, *12*(20). **https://doi.org/10.3390/app122010492**

Alias, M. F., Udin, W. S., & Piramli, M. K. (2022). High-Resolution Mapping Using Digital Imagery of Unmanned Aerial Vehicle (UAV) at Quarry Area, Machang, Kelantan. *IOP Conference Series: Earth and Environmental Science*, *1102*(1). **https://doi.org/10.1088/1755-1315/1102/1/012019**

Bulut, E., & Yılmaztürk, F. (2022). Investigation of the effects of different flight parameters on the accuracy of DEM generated using UAV systems. *Turkish Journal of Geosciences*, *3*(1), 22–29. **https://doi.org/10.48053/turkgeo.1114813**

Cho, J. W., Lee, J. K., & Park, J. (2021). Large-scale earthwork progress digitalization practices using series of 3D models generated from UAS images. *Drones*, *5*(4). **https://doi.org/10.3390/drones5040147**

Du, M., Li, H., & Roshanianfard, A. (2022). Design and Experimental Study on an Innovative UAV-LiDAR Topographic Mapping System for Precision Land Levelling. *Drones*, *6*(12). **https://doi.org/10.3390/drones6120403**

Elkhrachy, I. (2021). Accuracy Assessment of Low-Cost Unmanned Aerial Vehicle (UAV) Photogrammetry. *Alexandria Engineering Journal*, *60*(6), 5579–5590. **https://doi.org/10.1016/j.aej.2021.04.011**

Jiménez-Jiménez, S. I., Ojeda-Bustamante, W., Marcial-Pablo, M. D. J., & Enciso, J. (2021). Digital terrain models generated with low-cost UAV photogrammetry: Methodology and accuracy. *ISPRS International Journal of Geo-Information*, *10*(5). **https://doi.org/10.3390/ijgi10050285**

Liu, X., Lian, X., Yang, W., Wang, F., Han, Y., & Zhang, Y. (2022). Accuracy Assessment of a UAV Direct Georeferencing Method and Impact of the Configuration of Ground Control Points. *Drones*, *6*(2). **https://doi.org/10.3390/drones6020030**

Muhammad, M., & Tahar, K. N. (2021). Comprehensive Analysis of UAV Flight Parameters for High Resolution Topographic Mapping. *IOP Conference Series: Earth and Environmental Science*, *767*(1). **https://doi.org/10.1088/1755-1315/767/1/012001**

Muradás Odriozola, G., Pauly, K., Oswald, S., & Raymaekers, D. (2024). Automating Ground Control Point Detection in Drone Imagery: From Computer Vision to Deep Learning. *Remote Sensing*, *16*(5). **https://doi.org/10.3390/rs16050794**

Pathak, S., Acharya, S., Bk, S., Karn, G., & Thapa, U. (2024). UAV-based topographical mapping and accuracy assessment of orthophoto using GCP. *Mersin Photogrammetry Journal*, *6*(1), 1–8. **https://doi.org/10.53093/mephoj.1350426**

Quamar, M. M., Al-Ramadan, B., Khan, K., Shafiullah, M., & El Ferik, S. (2023). Advancements and Applications of Drone-Integrated Geographic Information System Technology—A Review. *Remote Sensing*, *15*(20), 1–35. **https://doi.org/10.3390/rs15205039**

Rábago, J., & Portuguez-Castro, M. (2023). Use of Drone Photogrammetry as An Innovative, Competency-Based Architecture Teaching Process. *Drones*, *7*(3), 1–18. **https://doi.org/10.3390/drones7030187**

Saifizi, M., Azani Mustafa, W., Syahirah Mohammad Radzi, N., Aminudin Jamlos, M., & Zulkarnain Syed Idrus, S. (2020). UAV Based Image Acquisition Data for 3D Model Application. *IOP Conference Series: Materials Science and Engineering*, *917*(1). **https://doi.org/10.1088/1757-899X/917/1/012074**

Santrač, N., Benka, P., Batilović, M., Zemunac, R., Antić, S., Stajić, M., & Antonić, N. (2023). Accuracy Analysis of UAV Photogrammetry Using RGB And Multispectral Sensors. *Geodetski Vestnik*, *67*(4), 459–472. **https://doi.org/10.15292/geodetski-vestnik.2023.04.459-472**

Syetiawan, A., Gularso, H., Kusnadi, G. I., & Pramudita, G. N. (2020). Precise topographic mapping using direct georeferencing in UAV. *IOP Conference Series: Earth and Environmental Science*, *500*(1). **https://doi.org/10.1088/1755-1315/500/1/012029**

Zolkepli, M. F., Ishak, M. F., & Daud, S. (2023). The Application of Unmanned Aerial Vehicle (UAV) For Slope Mapping at Gambang Damai Residents, Pahang: A Case Study. *International Journal of Integrated Engineering*, *15*(2), 219–227. **https://doi.org/10.30880/IJIE.2023.15.02.021**